

Spurious self-feedback of mean-field predictions inflates infection curves

Claudia Merger,^{1,2,*} Jasper Albers,^{1,2} Carsten Honerkamp,² and Moritz Helias^{1,2}

¹*Institute of Neuroscience and Medicine (INM-6) and Institute for Advanced Simulation (IAS-6) and JARA-Institute Brain Structure-Function Relationships (INM-10), Jülich Research Centre, Jülich, Germany*

²*RWTH Aachen University, Aachen, Germany*

(Dated: December 25, 2023)

The susceptible-infected-recovered (SIR) model and its variants form the foundation of our understanding of the spread of diseases. Here, each agent can be in one of three states (susceptible, infected, or recovered), and transitions between these states follow a stochastic process. The probability of an agent becoming infected depends on the number of its infected neighbors, hence all agents are correlated. A common mean-field theory of the same stochastic process however, assumes that the agents are statistically independent. This leads to a self-feedback effect in the approximation: when an agent infects its neighbors, this infection may subsequently travel back to the original agent at a later time, leading to a self-infection of the agent which is not present in the underlying stochastic process. We here compute the first order correction to the mean-field assumption, which takes fluctuations up to second order in the interaction strength into account. We find that it cancels the self-feedback effect, leading to smaller infection rates. In the SIR model and in the SIRS model, the correction significantly improves predictions. In particular, it captures how sparsity dampens the spread of the disease: this indicates that reducing the number of contacts is more effective than predicted by mean-field models.

I. INTRODUCTION

The Susceptible-Infected-Recovered (SIR) models and its variants [1] are highly popular models for the spread of diseases. They are built on the assumption that, to model the spread of a disease in a large population, the effect of each single individual is small. The stochastic SIR model instead describes the relative fractions of individuals that are in either of the three states, susceptible, infected, or recovered. Changes of these fractions are controlled by the average probability β of infecting a contact person and the average probability of recovery μ . One then assumes the same average transition rates between states for each individual, which only depend on the size of the relative fractions of the population in each states. Assuming homogeneous interactions between all individuals, and averaging over the stochastic process one arrives at a set of three coupled differential equations, which describe the average growth of the infection curve.

However, it has been demonstrated that the assumption of homogeneity of interactions across individuals and time is insufficient [2–7], and that real world propagation must be modeled using heterogeneous networks. One then describes a stochastic process of N agents, whose probability of infection depends on the number of infected nearest neighbors on a contact graph. This is also referred to as individual-based modeling (IBM) or agent-based modeling (ABM) [8]. Due to the interaction of all agents, the average growth of the infection curve cannot be computed. Under the assumption that the agents statistics are independent, one arrives at a set of $3N$ coupled update equations, the mean-field approximation of

the stochastic process that describe the average infection curve for each agent.

The mean-field equations are an insufficient approximation of the stochastic process, especially if the contact graph is sparse [2]. We will demonstrate this here by comparison to simulations of the same process, finding that mean-field predictions invariably overestimate the number of infected agents. The mismatch between the ground truth and its mean-field approximation is most prominent in sparse network structures. We then show that the predictions can be improved in a systematic manner using a dynamical Plefka expansion analogous to [9]. We treat both the SIR and SIRS model. The latter is a variant of the former. Here, agents may lose their immunity after recovery, so that multiple infections of the same agent are possible. In the case of the SIR model, the corrections obtained via this expansion cancel a spurious self-feedback effect: when an agent infects its neighbors, this infection may travel back to the original agent, leading to a self-infection of the agent at a later time. This self-feedback effect is present in the mean-field approximation of the model, but not in the underlying stochastic process. We show that the corrected equations can predict the dampening effect of sparsity both in the SIR and SIRS models. Additionally, computing the corrected theory is efficient, requiring one additional dynamical variable per node, such that the number of dynamical variables which one has to track still only scales with N .

Apart from the mean-field method, there exist further methods to approximate the dynamics. They are dynamical message-passing (DMP) [10, 11] and what is known as the pair approximation [12]. Both of these approaches yield a higher-dimensional set of coupled differential equations than mean-field. For DMP, one must track one dynamical variable per edge on the contact

* c.merger@fz-juelich.de

graph, for the pair approximation one must track one dynamical variable per pair of nodes, thus $\mathcal{O}(N^2)$ variables. We further discuss the relation of the fluctuation correction to DMP and the pair approximation in Section V.

This paper is organized as follows: in Section II, we introduce the SIR model and the most common approximation of the underlying stochastic process. In Section III, we present the fluctuation correction to the SIR model and its variants. We demonstrate the effect of the self-feedback term in Section IV. Finally we discuss our result in Section V.

II. SIR MODEL

We model N individuals i whose social contacts are represented by a graph with adjacency matrix a . Individuals may only transmit the disease to or be infected by their direct nearest neighbors on the graph. We assign to each individual a set of two binary variables, $S_i, I_i \in \{0, 1\}$. The susceptible state corresponds to $S_i = 1$ and $I_i = 0$, the infected state is defined by $S_i = 0$ and $I_i = 1$. Once an individual recovers, we set $S_i = I_i = 0$. All other configurations of S_i, I_i are not allowed. At each time step, the probability of infection of node i is $\phi(\theta_i)$ with the input θ_i to node i defined by

$$\theta_i(t) = h_i(t) + \beta \sum_j a_{ij} I_j(t) \quad (1)$$

with an external field $h_i(t)$ (corresponding to influx of infections from outside the network) and the interaction strength β , which increases the probability of an infected node infecting a susceptible one. We will later set $h_i = 0$ to investigate the endogenous dynamics. In principle, $\phi : [0, \infty) \rightarrow [0, 1]$ can be any function which maps to a probability. We will further assume that, close to the origin, ϕ is well approximated by the identity, such that $\phi(0) = 0$, and $\phi'(0) = 1$. The standard formulation of the SIR model defines $\phi(\theta) = \theta$, which we will adopt here and in the following. In this case, the interaction strength β is just the probability of an infected node transmitting the disease to one of its nearest neighbors. An infected individual recovers in each time step with probability μ .

In the SIRS model, a variant of the SIR model with waning immunity, recovered individuals may move back to the susceptible state with probability η . An overview of the transition probabilities between the compartments is shown in Fig. 1.

The model is a stochastic Markov process because transitions take place randomly with the transition probabilities defined above and, given the current state, the evolution is history independent. We denote as $\langle \dots \rangle$ the expectation value over this randomness. Because the state variables S_i and I_i are binary $\in \{0, 1\}$, their expectation values $\langle S_i \rangle =: \rho_i^S$ and $\langle I_i \rangle =: \rho_i^I$ equal the probabilities to occupy the corresponding state, S or I , respectively. We are interested in the evolution of these probabilities

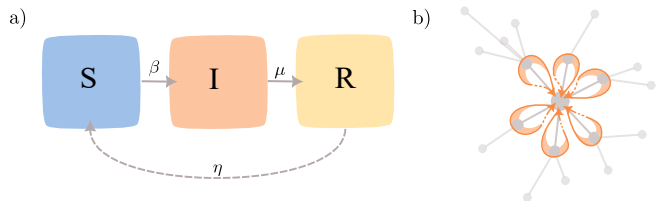


Figure 1. a) Transition probabilities in the SIR (solid lines) and SIRS (solid and dashed lines) model. b) Illustration of self-feedback.

ρ_i^α that individual i is in state $\alpha \in \{S, I, R\}$. Taking all possible transitions together, we may write down the difference $\Delta \rho_i^\alpha(t+1) = \rho_i^\alpha(t+1) - \rho_i^\alpha(t)$ between to time steps exactly:

$$\begin{aligned} \Delta \rho_i^S(t+1) &= \eta \rho_i^R(t) - \langle S_i(t) \theta_i(t) \rangle \\ \Delta \rho_i^I(t+1) &= -\mu \rho_i^I(t) + \langle S_i(t) \theta_i(t) \rangle. \end{aligned} \quad (2)$$

These update equations can be seen as a balance of probability influx and outflux from the states: individuals enter the susceptible from the recovered state with probability η , which yields the first term in $\Delta \rho_i^S(t+1)$. On the other hand, individual agents leave the state if they become infected which happens with probability $\langle S_i(t) \theta_i(t) \rangle$, which may be interpreted as the product of the probability θ_i to become infected given the individual is susceptible times the probability to be susceptible. This gives us the second term in $\Delta \rho_i^S(t+1)$ and the second term in $\Delta \rho_i^I(t+1)$. Infected agents leave the infected state with the probability μ for recovery, which accounts for the first term in $\Delta \rho_i^I(t+1)$. Here and in the following, setting $\eta = 0$ yields the evolution for the SIR model. It is sufficient to track only ρ_i^I and ρ_i^S since ρ_i^R follows from $\rho_i^R = 1 - \rho_i^S - \rho_i^I$.

The difficulty in evaluating Eq. (2) lies in computing the expectation value $\langle S_i(t) \theta_i(t) \rangle$, for which we must compute the cross-correlations between individuals for all times. As the system size grows, an evaluation of the exact update equations for ρ_i^α becomes computationally infeasible. A typical approximation stipulates that individuals are statistically independent, meaning that averages of the type $\langle S_i(t) \theta_i(t) \rangle$ factorize into $\langle S_i(t) \rangle \langle \theta_i(t) \rangle$, since θ_i neither depends on S_i nor I_i . This yields the individual-based mean-field equations:

$$\begin{aligned} \Delta \rho_i^S(t+1) &= \eta \rho_i^R(t) - \rho_i^S(t) \beta \sum_j a_{ij} \rho_j^I(t) \\ \Delta \rho_i^I(t+1) &= -\mu \rho_i^I(t) + \rho_i^S(t) \beta \sum_j a_{ij} \rho_j^I(t), \end{aligned} \quad (3)$$

which, apart from replacing $\langle S_i(t) \theta_i(t) \rangle$ by $\rho_i^S(t) \beta \sum_j a_{ij} \rho_j^I(t)$, are equal to Eq. (2). We will refer to them simply as mean-field equations in the following. Given initial expectation values $\rho_i^\alpha(0)$, these equations can then be iterated to compute the prediction for the average infection curve. However, we will show

in the following that the assumption of statistical independence is not well-justified. Note that in Eq. (3), the probability of a nearest neighbor of node i being infected, $\rho_j^I(t)$ contains the term $\rho_j^S(t-1)\beta a_{ji}\rho_i^I(t-1)$, which then contributes to the probability of node i being infected two time steps later. In the next section, we will see that this term is canceled by fluctuations.

III. CANCELLATION OF SELF-FEEDBACK

Indeed, we find that correlations do play a role. We show in Appendix B that the mean-field Eqs. (3) can be obtained as a first order approximation in β from a systematic fluctuation expansion: we extend the individual-based mean-field equations by performing a Plefka expansion [13] to second order. In [9], Roudi and Hertz demonstrated how to do the Plefka expansion in the dynamical setting for a system of Ising spins. The resulting update equations are also known as dynamical TAP equations, a non-equilibrium version of the so-called TAP correction term [14], first derived in [15]. Our calculation closely follows [9], with the important distinction that here the transition probability between states depends on the state itself. The terms in the expansion are ordered by powers of β , hence we expand around the point where $\beta = 0$, in which case the independence of individuals is exact, and the model can be solved exactly. To first order, one obtains Eqs. (3), and to second order, each update equation acquires a correction term of order β^2 , which reads

$$\begin{aligned}\Delta\rho_i^S(t+1) &= \eta\rho_i^R(t) - \rho_i^S(t)\beta\sum_j a_{ij}(\rho_j^I(t) - \rho_{j\leftarrow i}^I(t)), \\ \Delta\rho_i^I(t+1) &= -\mu\rho_i^I(t) + \rho_i^S(t)\beta\sum_j a_{ij}(\rho_j^I(t) - \rho_{j\leftarrow i}^I(t)),\end{aligned}\quad (4)$$

where $\rho_{j\leftarrow i}^I(t)$, to first order in β , is just the probability that node j was infected by node i at an earlier point in time and stayed in this state since then,

$$\rho_{j\leftarrow i}^I(t) := \beta a_{ji} \sum_{t'\leq t-1} \rho_j^S(t')\rho_i^I(t')(1-\mu)^{t-t'-1}.$$

Here, $\rho_i^I(t')\beta a_{ji}\rho_j^S(t')$ describes the probability that node j becomes infected at $t'+1$ due to node i , and $(1-\mu)^{t-t'-1}$ is the probability that node j does not recover between $t'+1$ and t . We find that the second order correction therefore is exactly the term which cancels the self-feedback of i onto itself to first order in β . In the SIR model, this cancellation is necessary, since in the stochastic process, any individual can either be susceptible or infected, and nothing in between. Therefore, once an individual has been infected, this infection may not travel back and re-infect the individual, since the transitions $I \rightarrow S$ and $R \rightarrow S, R \rightarrow I$ have probability zero. Alternatively, one may view approximations leading to Eqs. (3)

as artificially introducing a positive self-feedback, which is not present in the underlying stochastic process.

We performed the expansion to second order for the SIR, SIRS, and the SIS model (see Appendix B and Appendix C). In the latter, no recovered state exists, rather infected agents move to the susceptible state again with probability $\bar{\mu}$. Here and in the following, we analyze only the SIR and SIRS model, an overview of the corrected dynamical equations including the SIS model is found in Appendix A.

IV. DAMPENING EFFECT OF SPARSITY

We will now compare the predictions of Eqs. (3) to the corresponding results from Eqs. (4) on different network topologies. We implement simulations of the SIR and SIRS dynamics using NEST [16], a simulator for spiking neural networks, which we adapt to encode transitions between binary states, see Appendix D. The mean-field and TAP predictions were obtained by iterating the update equations, see Appendix E.

1. SIR model

We here study the effect which the average connectivity has on the spread of the infection. To do so, we generate random regular graphs of different degree k per node, infect a small fraction (5%) of randomly chosen agents, and then let the dynamics evolve. Random regular graphs possess no hierarchical structure: all nodes have equal degree, and their connections are chosen at random. Hence, they are suited to study the effect of the average connectivity on the spread of the infection.

We compare the predictions of the mean-field and second-order approximation to simulations of the stochastic process. In Fig. 2 (a)-(c) we show the infection curves, averaged over the whole population, as well as a small example graph on the left hand side. (Note that for $k = 2$, graphs typically consist of periodic linear chains.) For densely connected networks, the predictions of mean-field theory, the second order correction and the simulation all agree. As the networks become more sparse, however, the number of infections decreases much faster than mean-field theory predicts, but is still well approximated by the second order corrected theory. This shows that self-feedback is highly relevant for sparse networks.

The latter observation holds true over a broad range of fractions $\lambda = \frac{\beta}{\mu}$. After the infection wave has died down, all agents must be either susceptible or recovered. As we report in Fig. 2 (d), the number of susceptible agents in the final state, ρ_∞^S , decreases with increasing λ – but much slower than predicted by mean-field theory. We find that, on sparse graphs in particular, the difference between the mean-field prediction and the simulation is large, while (4) captures the dynamics well.

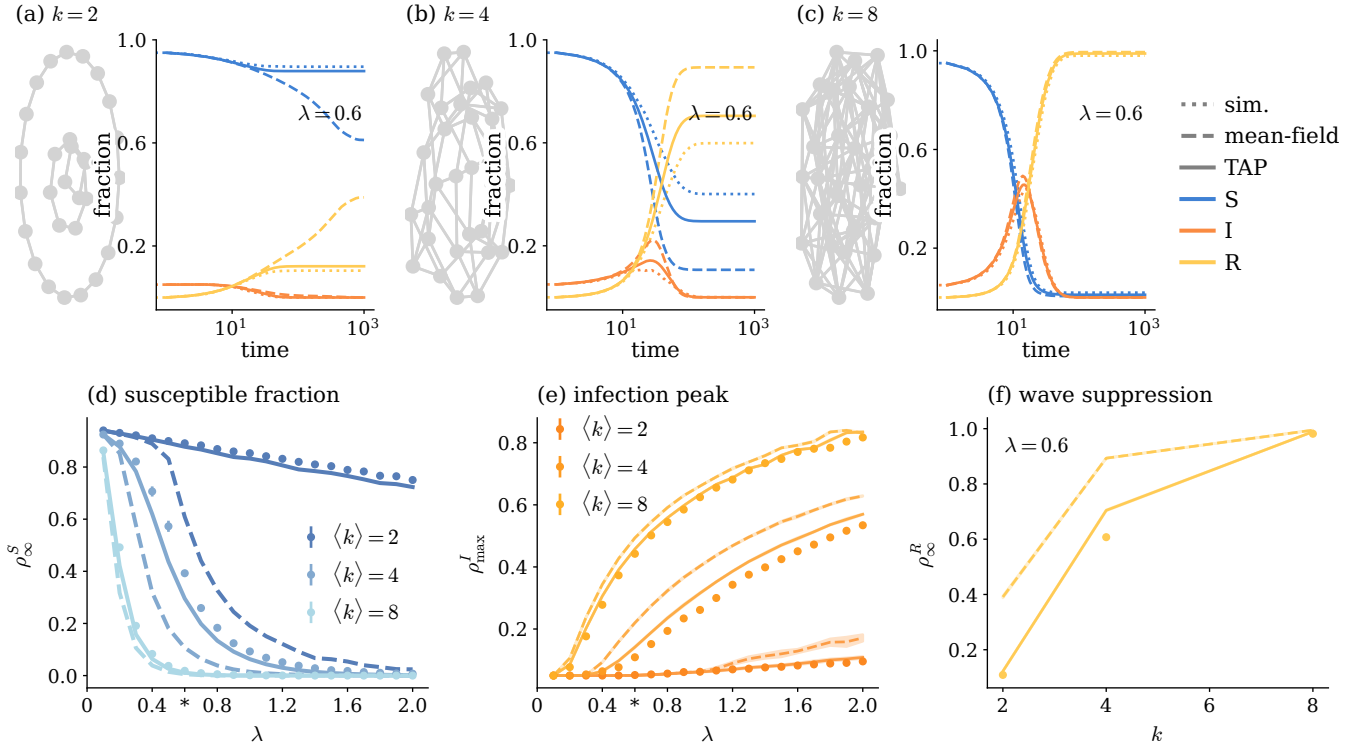


Figure 2. **Sparsity suppresses spread of infection in the SIR model on random regular networks.** (a)-(c) Dotted curves show simulation results for fixed $\mu = 10^{-1}$, and $\lambda := \frac{\beta}{\mu} = 0.6$, shaded areas show one standard deviation, averaged over 10 different realizations of the stochastic infection process on the same network realization with the same initially infected agents. Dashed curves show mean-field result; solid curves the prediction from the TAP equations, the second order correction. (d) Fraction of agents in the susceptible state after the dynamics have stopped. Dots are simulation results, curves show mean-field and TAP, shaded areas indicate one standard deviation. (e) Same as (d), but for the peak of the infection curve. Stars along the axis mark the value of λ used in (a)-(c). (f) Fraction of agents in the recovered state after the dynamics have stopped over the degree k of the network. All results were obtained on networks with average size $N = 10^3$. All data in (d)-(f) are averaged over 10 realizations of the adjacency matrix, results in (a)-(c) stem from a single realization of the adjacency matrix.

Finally, we compare the height of the peak for different network topologies and different values of λ in Fig. 2 (e). We find that below a certain value of λ , which depends on the degree k , the number of infected individuals does not grow beyond the number of initially infected agents, thus the infection wave dies out immediately. Beyond this point, the height of the infection peak increases with λ . Again, the mean-field theory predicts a higher value than observed in simulations. We find that the number of infected agents overall decreases rapidly with the average degree. After the dynamics have stopped, the number of recovered agents is equivalent to the overall number of agents that experienced an infection. In Fig. 2(f), we compare the fraction ρ_∞^R of recovered agents after the infection wave has died out to predictions from both theories, finding again that as the graph becomes sparser, far fewer agents become infected than predicted by mean-field theory.

Despite the good agreement between simulations and

the second-order correction Eq. (4), we find that the corrected theory consistently overestimates the fraction of infected agents slightly, both at the height of the wave, as shown in Fig. 2 (e), and in the average over the time trajectory see Fig. 2 (d). This is so, because the correction Eq. (4) still allows higher order feedback loops. Nevertheless, in comparison to the difference between mean-field theory and the second order correction, these higher-order terms appear to play a minor role.

In conclusion, the analysis confirms that sparser connectivity has a more pronounced effect than mean-field theory suggests: The activity dies out faster and its peak is much lower, hence the number of individuals which have ever been infected is more strongly suppressed by a reduction in the number of contacts.

2. SIRS model

In the SIRS model, an infected agent can reach the susceptible stage again. Hence, in principle, a self-infection loop is allowed, provided that the transition back to the susceptible state has taken place in the meantime. Given this, the correction Eq. (4) seems counter-intuitive: clearly, self-feedback may exist in the SIRS model, but the correction appears to cancel it. However, the allowed self-feedback loop in the SIRS model must come with a factor of η , which appears neither in the spurious self-feedback term in mean-field theory, nor in the correction in Eq. (4). The cancellation in Eq. (4) is only partial; higher order terms may indeed constitute self-feedback in the corrected update equations.

In contrast to the SIR model, an endemic state, which is a state with finite activity ($\rho^I > 0$), can emerge in the SIRS model; then the infection wave does not die out fully, rather, at all times, a finite fraction of the population is infected. The fraction λ_c , which marks the transition between the regimes where the activity dies out or remains finite, is called the epidemic threshold. In Appendix F, we derive an estimator for this regime from Eq. (4) and apply it to scale-free networks, a class of strongly heterogeneous networks, in Appendix G. Here, we again focus on the effect of the average connectivity, and investigate the spread of disease on random regular networks. We apply Eq. (4) to a system with slowly waning immunity; setting $\mu = 10^{-1}$, $\eta = 10^{-2}$ and varying β between η and 2μ . We show the results of this procedure in Fig. 3.

We find that the fluctuation correction reproduces the average dynamics well (see Fig. 3 (a) - (c)). In particular, in the sparse connectivity model, the infection wave dies out completely, which is accurately predicted by the fluctuation correction, whereas mean-field theory predicts an endemic state with large connectivity. For large connectivity, the difference between mean-field and fluctuation correction is also small; both overestimate the number of infections slightly. The height of the infection peak is predicted with high accuracy by the fluctuation correction at all levels of connectivity (see e Fig. 3 (d)), while it is overestimated by the mean-field result, especially for sparse graphs. For intermediate and dense connectivity, here $k = 4$ and $k = 8$, we find that strong fluctuations emerge in the dynamics, which are modeled neither by mean-field, nor by the TAP equations. However, the fluctuation correction overestimates the activity in the endemic state: it underestimates the final fraction of susceptible individuals, while it overestimates the number of infected agents in the final epidemic state, see Fig. 3 (c), (d).

Fixpoints For long time scales, we observe that the activity in the SIRS model typically does not converge to zero. We here investigate the onset of this regime using a simplified version of the dynamical equations Eq. (3), Eq. (4), where we set the left hand side to zero $\Delta\rho^\alpha = 0$. Solutions to these equations are therefore fixpoints of the average dynamics. Finding a fixpoint where $\rho^I \neq 0$

corresponds to a state with finite activity in the system at all times. We may then drop the time dependence, since by construction solutions to the fixpoint equations no longer evolve. We further propose a solution where all nodes have equal probability of being in state α ,

$$\rho_i^\alpha = \bar{\rho}^\alpha \quad \forall i. \quad (5)$$

This solution should be attained only in networks which are sufficiently homogeneous. In random regular networks, although they are not as homogeneous as, e.g., a 2d square grid, all nodes have equal degree. Thus, under the assumption that Eq. (5) holds, sums over nearest neighbors of nodes simplify, $\sum_j a_{ij}\rho_j^I \rightarrow k_i\bar{\rho}^I$, with k_i the degree of the i -th node, which is equal to k for all i in random regular networks. The mean-field solution to the homogeneous fixpoint-equations is then

$$\bar{\rho}_{\text{MF}}^I \in \left\{ 0, \frac{\eta}{\eta + \mu} \left(1 - \frac{1}{\lambda k} \right) \right\}. \quad (6)$$

The trivial solution, $\bar{\rho}_{\text{MF}}^I = 0$, always exists. Since we must have $\bar{\rho}_{\text{MF}}^I \geq 0$, the non-trivial solution emerges as soon as $\lambda \geq \lambda_c^{\text{MF}} := k^{-1}$.

To derive a similar prediction for the TAP equations, we introduce another dynamical variable $\tau_i(t) = \sum_j a_{ij}\rho_{j \leftarrow i}^I(t)$. We then find

$$\Delta\tau_i(t+1) = -\mu\tau_i(t) + \beta \sum_j a_{ij}a_{ji}\rho_j^S(t)\rho_i^I(t) \quad (7)$$

and we can replace the term $\beta \sum_j a_{ij}\rho_{j \leftarrow i}(t)$ by $\tau_i(t)$ in Eq. (4). An explicit statement of all evolution equations using τ is given in Appendix A. We now make the same homogeneity assumption, set $\Delta\bar{\rho}^\alpha = 0$, $\Delta\bar{\tau} = 0$ and drop the time arguments. This yields the conditions

$$\begin{aligned} \rho^R &= \frac{\mu}{\eta} \bar{\rho}^I \\ 0 &= -\mu\bar{\rho}^I + \bar{\rho}^S \beta k \bar{\rho}^I - \bar{\rho}^S \beta \tau \\ 0 &= -\mu\tau + \bar{\rho}^I \beta k \bar{\rho}^S. \end{aligned}$$

Thus, we obtain a cubic equation in $\bar{\rho}^S$ with the solutions

$$\bar{\rho}_{\text{TAP}}^S \in \left\{ 1, \frac{1}{2\lambda} \left(1 \pm \sqrt{1 - \frac{4}{k}} \right) \right\},$$

For $k < 4$, we find only the trivial solution $\bar{\rho}^S = 1$. For $k \geq 4$, a non-trivial solution emerges as soon as $\lambda \geq \lambda_c^{\text{TAP}} := \frac{1}{2} \left(1 - \sqrt{1 - \frac{4}{k}} \right)$. We here choose the solution with the minus sign as this yields the lowest λ at which $\bar{\rho}_{\text{TAP}}^S < 1$ holds. Note that for $k \gg 4$, this again reproduces the mean-field result $\lambda_c^{\text{TAP}} \approx k^{-1} + \mathcal{O}\left(\left(\frac{4}{k}\right)^2\right)$. The corresponding curves for $\bar{\rho}^I$ read

$$\bar{\rho}_{\text{TAP}}^I \in \left\{ 0, \frac{\eta}{\eta + \mu} \left(1 - \frac{1}{2\lambda} \left(1 \mp \sqrt{1 - \frac{4}{k}} \right) \right) \right\}. \quad (8)$$

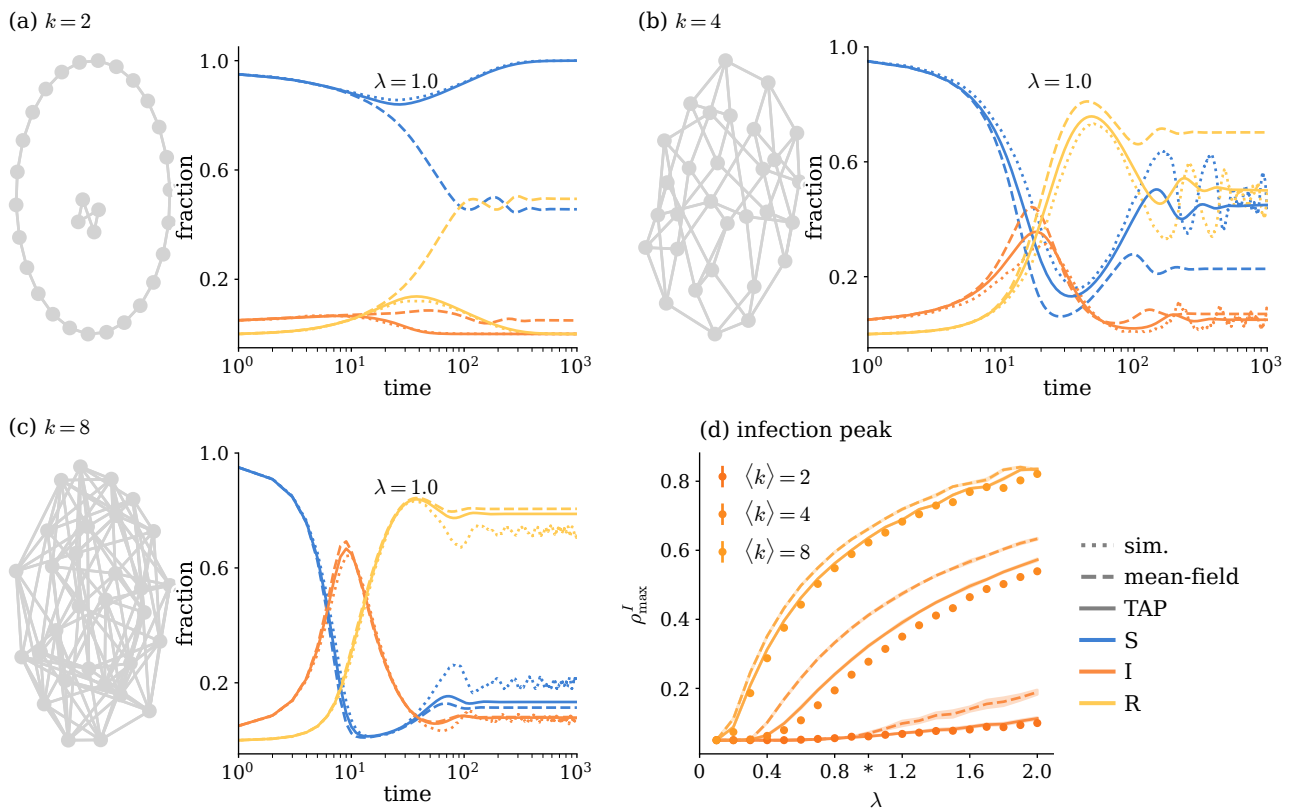


Figure 3. **Fluctuation correction for SIRS model on random regular networks with slowly waning immunity at system size $N = 10^3$.** (a)-(c) Dotted curves show results of simulations for fixed $\mu = 10^{-1}$, $\eta = 10^{-2}$, and $\lambda = 1.0$, shaded areas show one standard deviation, averaged over the surviving runs of 10 different realizations of the stochastic process on the same network realization with the same initially infected agents. Dashed curves show mean-field result; solid curves the prediction from TAP equations, the second order correction. (d) Peak of the infection curve, averaged over all runs (surviving- and non-surviving). Dots show simulation result (error bars are typically smaller than marker size). Dashed curves show the peak of the mean-field prediction, solid curves the peak of the correction. All data in (d) are averaged over 10 realizations of the adjacency matrix. Stars along the x-axis mark the value of λ used in (a)-(c).

it is interesting to observe that the curve for $\bar{\rho}_{\text{MF}}^I$ for $k = 2$ thus coincides with the corresponding curve $\bar{\rho}_{\text{TAP}}^I$ for $k = 4$. This means that the TAP prediction yields the same endemic state, at double connectivity for this special configuration. This illustrates the impact sparsity on the dynamics.

We compare these predictions to simulations on random regular graphs in Fig. 4. First, we verify that the simplified Eqs. (6), (8) indeed match the outcome of the full update Eqs. (3) and (4). This is shown in Fig. 4(a). We also find that the mean-field prediction for $k = 2$ indeed coincides with the corresponding curve for the TAP prediction at $k = 4$.

We then average the outcome of the simulation for ρ^I over the last 500 time steps, and compare this result to mean-field and TAP theory for varying λ and k in Fig. 4 (b) and (c). Again, we find a better agreement between TAP theory and the simulation. In particular, TAP theory accurately predicts vanishing activity at $k < 4$. However, TAP theory still overestimates the average activity

slightly both in the dynamics (see e.g. Fig. 3(c)) and in the endemic state (e.g. predicting a non-vanishing contribution at $\lambda \approx 0.7$ and $k = 4$ in Fig. 4(b)). If the mechanism which leads to the deviation between the fluctuation correction and the simulation were the omission of the positive self-feedback loop which we described at the outset of this section, then the fraction of infected agents in the endemic state should be underestimated by the fluctuation correction. Contrary to this, we rather find that it is overestimated by the fluctuation correction.

V. DISCUSSION

We have demonstrated that a fluctuation correction to the SIR equations cancels a spurious self-feedback effect, which leads to inflated infection curves in the standard mean-field version of the SIR model. As a result, we find that the updated model not only correctly predicts a significantly lower peak of infection, but also a far larger

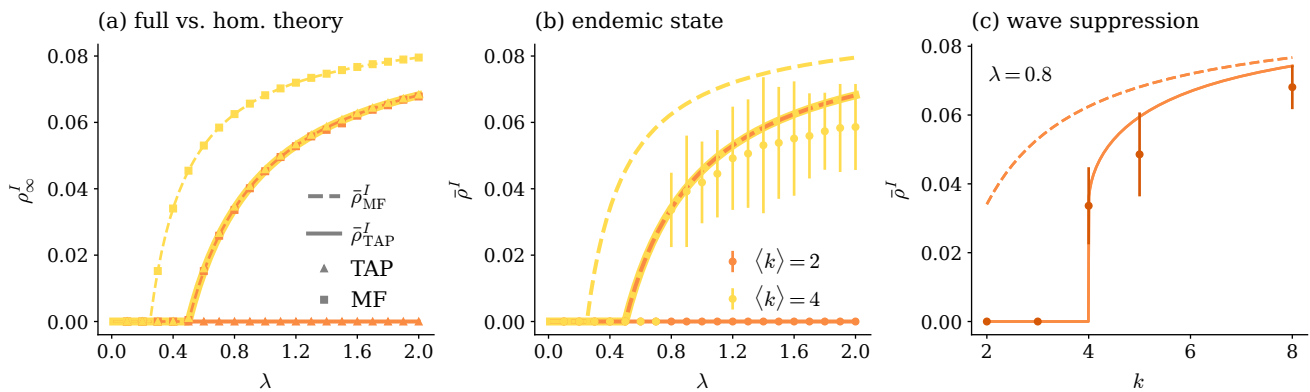


Figure 4. **Endemic state in the SIRS model on random regular networks with slowly waning immunity**, $\eta = 10^{-2}$, **and system size** $N = 10^3$. **(a)** Comparison of theoretical prediction for fraction of infected agents at equilibrium for degree $k = 2$ (orange) and $k = 4$ (yellow). Triangles and squares show the outcome of the mean-field theory (Eqs. (3)) and TAP theory (Eqs. (4)), respectively. Dashed and solid curves show theoretical results under the assumption of homogeneity, Eqs. (6) and (8), respectively. Results from TAP theory for $k = 4$ overlap with results from mean-field theory for $k = 2$. **(b)** Dashed and solid curves show theoretical results under the assumption of homogeneity. Dots are simulation results averaged over surviving runs and 10 realizations of the adjacency matrix. Additionally, to mitigate the effect of oscillations, results were averaged over the last 500 steps of the simulation, comp. Fig. 3. **(c)** Same as (b), but for fixed $\lambda = 0.8$ and varying degree k .

fraction of susceptible *and therefore never infected* individuals in the final endemic state. This shows that there exists an important distinction between the stochastic process and the mean-field approximation of the former process. Classical SIR models hence represent a different process, in which self-feedback is present.

Note that the correction term in Eq. (4) only cancels self-feedback up to second order in β . The expansion outlined in Appendix B can be extended to higher order corrections, which may also include higher order effects such as self-feedback effects along loops of the network, e.g. contributions $\propto \beta^3 a_{ij} a_{jk} a_{ki}$, corresponding to a self-feedback term along the loop from i to j to k and then back to i . This may be relevant for network topologies with large clustering coefficients. Furthermore, we have assumed the network connectivity to be constant; however the theoretical framework allows for a time dependence of the connectivity matrix as well. We leave an investigation of higher order corrections and network temporal variations of the connectivity to future work.

Numerous studies have previously demonstrated that network heterogeneity plays an important role in the predictions of the SIR model [2–7]. In particular, Thurner et al. [2] reported a large difference between the completely homogeneous SIR model and a simulation of the stochastic process, which they attribute to the network topology. The correction effect we describe here is relevant for all network topologies, but increasingly so for sparser networks. In particular, the correction for self-feedback shows that reducing the number of contacts, thus causing sparser network topology, has a stronger effect than standard SIR calculations suggest, and is therefore an even more effective measure to suppress the spread of disease than previously assumed.

Other than the mean-field approximation both the pair approximation [12] and dynamical message passing (DMP) [10, 11] have emerged as approximations of the stochastic process. Within the pair-approximation [17, 18], not to be confused with the “independent pair approximation”, see e.g. [19], in addition to the first moments, one also takes pairwise correlations between agents into account. However, the evolution of first and second moments of the distribution is not closed, to compute their time evolution, one needs to compute third moments, which are then approximated using second and first moments. While the pair approximation certainly improves upon the mean-field equations, it is less computationally efficient, requiring the tracking of $\mathcal{O}(N^2)$ coupled differential equations. In contrast, in our framework we must only track $\mathcal{O}(N)$ dynamical variables.

Within the SIR model, self-feedback is forbidden, since the transitions $I \rightarrow S$ and $R \rightarrow S, I$ never occur. This idea of the cancellation of self-feedback in the SIR model underlies DMP: within DMP, one tracks messages, namely the probabilities that an infection is passed along a given edge of the graph. The DMP equations follow from a strict prohibition of all self-feedback. The number of dynamical variables tracked in the DMP approach scales with the number of edges. For the SIR model, DMP is exact on trees.

Within variants of the SIR model where transitions back to the susceptible state are allowed, such as the SIS or SIRS model, self-feedback may indeed occur, see e.g. [20–23]. Nevertheless, the authors of [24] applied recurrent DMP equations to the SIRS model, and found that eliminating self-feedback can lead to improved predictions. While a positive self-feedback loop is certainly present in these systems [23], the fluctuation correction

to the SIRS and SIS models has the same functional form as the one to the SIR model, hence it cancels a self-feedback effect up to the second order in the interaction strength. However, while the DMP approach heuristically imposes the non-existence of self-feedback, here its cancellation emerges from a systematic expansion. Furthermore, while the DMP equations of [24] eliminate all self-feedback, our update equations in principle allow for self-feedback of higher orders.

Within recurrent infection models, the allowed self-feedback loop, in which an initially infected node recovers and becomes susceptible again between the original infection and the reception of the self-feedback signal, comes with a factor $\beta^2\mu\eta \ll \beta^2$ for the SIRS model, or a factor $\beta^2\bar{\mu} \ll \beta^2$ for the SIS model. In the case in which the loss of immunity is significantly slower than the spread of infection, one could attempt to argue that this effect becomes negligible, thus justifying the use of DMP. However, depending on the network topology, the positive self-feedback effect exists, and can considerably change the predictions [23]. A systematic comparison between the pair approximation and the DMP approach to the SIRS model on scale-free graphs has been provided in [25]. The authors of the latter study find that neither theory predicts both the endemic activity and the localization of the activity above the epidemic threshold it accurately.

We found that even in systems where a positive self-feedback is in principle permitted, fluctuations can partially cancel the self-feedback effect. This observation can explain why an elimination of all self-feedback effects, reported in [24] via dynamic message passing, can yield improved results, even in systems where positive self-feedback loops are allowed. However, our results do not justify the complete cancellation of all self-feedback, which is known to lead to incorrect predictions [23]. Rather, our theory presents a middle ground between a complete elimination of the self-feedback effect and its over-representation in mean-field theory.

For the SIR model our result eliminates the strongest self-feedback effect, while it does not eliminate self-feedback altogether. For recurrent infection models such as the SIRS model, this partial elimination must be viewed in a different light: there, it is only a correction on the level of fluctuations. From the form of this correction term, we cannot conclude that self-feedback in all forms is absent in SIRS or SIS models. Nevertheless,

it can explain the partial success of DMP theory also in recurrent infection models, since it illustrates that fluctuations can lead to a cancellation of self-feedback to a certain extent. We expect that higher than second order corrections to the dynamics will differ in their nature depending on which variant of the three models one chooses.

We have found that both spin systems at equilibrium and disease models, can be linked via the same expansion method. It is interesting to observe that additionally, the expansion produces the cancellation of self-feedback in both models at second order. We have demonstrated that the expansion method can be applied also to other variants of the SIR model. This can be further extended, by incorporating for example the SEIR or SEIRS model. Moreover, the computation of higher-order corrections is straightforward.

Overall, it is usually possible to argue whether self-feedback should be present or absent in a system without a systematic fluctuation expansion, and the presence or absence of the same effect can have dramatic effects on the system's behavior. However, such a heuristic argument is not always sufficient to predict properties of the system as we saw in SIRS model. In particular, the non-cancellation of self-feedback does not imply that a first order mean-field theory is accurate. In these cases, a systematic fluctuation expansion can yield improved predictions. Computing these corrections in different systems in which self-feedback is allowed is an interesting direction of further research.

ACKNOWLEDGMENTS

This work was partly supported by the German Federal Ministry for Education and Research (BMBF Grant 01IS19077B to Aachen) and by NeuroSys as part of the initiative "Clusters4Future", which is funded by the Federal Ministry of Education and Research BMBF (03ZU1106CB). It was also partly supported by the European Union's Horizon 2020 Framework Programme for Research and Innovation under Specific Grant Agreement No. 945539 (Human Brain Project SGA3). We acknowledge funding by the Deutscher Akademischer Austauschdienst - DAAD scholarship programme "Forschungsstipendien für Doktorandinnen und Doktoranden 2022/2023" (DAAD, funding programme 57595573).

Appendix A: Evolution equations for SIR, SIRS, and SIS model

In Table I, we present the corrected evolution equations for all three models separately. Analogous to Section IV, we will introduce another dynamical variable τ_i to account for the TAP term; this makes it possible to implement the TAP evolution equations as $3N$ coupled update equations.

model	evolution equations
SIR	$\begin{aligned} \Delta \rho_i^S(t+1) &= -\rho_i^S(t)\beta \left(\sum_j a_{ij}\rho_j^I(t) - \tau_i(t) \right) \\ \Delta \rho_i^I(t+1) &= -\mu\rho_i^I(t) + \rho_i^S(t)\beta \left(\sum_j a_{ij}\rho_j^I(t) - \tau_i(t) \right), \\ \Delta \tau_i(t+1) &= (1-\mu)\tau_i(t) + \beta \sum_j a_{ji}\rho_j^S(t)\rho_i^I(t) \end{aligned}$
SIS	$\begin{aligned} \Delta \rho_i^S(t+1) &= \bar{\mu}\rho_i^I(t) - \rho_i^S(t)\beta \left(\sum_j a_{ij}\rho_j^I(t) - \tau_i(t) \right) \\ \Delta \rho_i^I(t+1) &= -\bar{\mu}\rho_i^I(t) + \rho_i^S(t)\beta \left(\sum_j a_{ij}\rho_j^I(t) - \tau_i(t) \right), \\ \Delta \tau_i(t+1) &= (1-\bar{\mu})\tau_i(t) + \beta \sum_j a_{ji}\rho_j^S(t)\rho_i^I(t) \end{aligned}$
SIRS	$\begin{aligned} \Delta \rho_i^S(t+1) &= \eta \left(1 - \rho_i^I(t) - \rho_i^S(t) \right) - \rho_i^S(t)\beta \left(\sum_j a_{ij}\rho_j^I(t) - \tau_i(t) \right) \\ \Delta \rho_i^I(t+1) &= -\mu\rho_i^I(t) + \rho_i^S(t)\beta \left(\sum_j a_{ij}\rho_j^I(t) - \tau_i(t) \right), \\ \Delta \tau_i(t+1) &= (1-\mu)\tau_i(t) + \beta \sum_j a_{ji}\rho_j^S(t)\rho_i^I(t) \end{aligned}$

Table I. Update equations of the TAP theory for the three models.

Appendix B: Expansion of the effective action for quenched disorder

We perform the fluctuation expansion analogous to [9], with an adapted transition probability. We use a short-hand notation

$$X_i(t) = \begin{pmatrix} S_i(t) \\ I_i(t) \end{pmatrix} \in \left\{ \begin{pmatrix} 1 \\ 0 \end{pmatrix}, \begin{pmatrix} 0 \\ 1 \end{pmatrix}, \begin{pmatrix} 0 \\ 0 \end{pmatrix} \right\}$$

to describe the state of each individual, and $X(t)$ to indicate the state of the whole system of nodes at each time point. At each time step, for each node we hence have a transition probability from $S_i(t), I_i(t)$ to $S_i(t+1), I_i(t+1)$

$$\begin{aligned} W_{t+1,t}[X(t+1)|\theta(t), X(t)] &= \prod_{i=1}^N W_{t+1,t}[X_i(t+1)|\theta_i(t), X_i(t)] \\ &= \prod_{i=1}^N \{ S_i(t+1) [1 - \phi(\theta_i(t))] S_i(t) \\ &\quad + I_i(t+1) [(1-\mu)I_i(t) + \phi(\theta_i(t)) S_i(t)] \\ &\quad + (1 - S_i(t+1) - I_i(t+1)) [1 - S_i(t) - (1-\mu)I_i(t)] \} . \end{aligned} \quad (\text{B1})$$

The first line corresponds to the individual remaining susceptible. The second corresponds to a new or sustained infection. The last line corresponds to the probability that the individual enters or remains in the recovered state. We start by defining a cumulant generating function

$$\mathcal{W}(\psi, h) = \ln \langle \exp(\psi^T X) \rangle \quad (\text{B3})$$

which couples a set of sources

$$\psi_i(t) = \begin{pmatrix} \psi_i^S(t) \\ \psi_i^I(t) \end{pmatrix}$$

to the fields, where we used the shorthand notation $\psi^T X = \sum_{i,t} \psi_i^T(t) X_i(t)$. The right hand side Eq. (B3) depends on the external fields h , since this alters the update probability $W_{t+1,t}[X(t+1)|\theta(t), X(t)]$ via θ , see Eq. (1).

One can compute the cumulants of the vectors $X_i(t)$, by taking the derivatives of Eq. (B3) by the sources ψ and subsequently setting $\psi = 0$. For example, we may obtain ρ_i^α by computing

$$\rho_i^\alpha(t) = \langle X_i^\alpha(t) \rangle = \partial_{\psi_i^\alpha(t)} \mathcal{W}(\psi, h) \Big|_{\psi=0} . \quad (\text{B4})$$

We may express the average in Eq. (B3), by enforcing the definition of the input fields θ via a Dirac delta distribution

and using that, conditioned on the input fields $\theta(t)$, the transitions from t to $t+1$ are independent across nodes

$$\begin{aligned} \langle \exp(\psi^\top X) \rangle_h = \sum_X p(X(0)) \prod_{i,t} \int \frac{d\theta_i(t) d\hat{\theta}_i(t)}{2\pi} \exp(\psi_i^\top(t) X_i(t)) \\ \cdot W_{t+1,t} [X_i(t+1) | \theta_i(t), X_i(t)] \\ \cdot \exp \left(i\hat{\theta}_i(t) \left[\theta_i(t) - h_i(t) - \beta \sum_j a_{ij} I_j(t) \right] \right) \end{aligned} \quad (\text{B5})$$

Here, we introduced an auxiliary field $\hat{\theta}_i(t)$ to enforce the condition Eq. (1) on $\theta_i(t)$ via the inverse Fourier transform $\delta(x) = \int \frac{dx}{2\pi} \exp(ixx)$. The sum \sum_X runs over all trajectories, i.e. all combinations of all configurations X across time $t \in \{0, \dots, T\}$. We must also average over the starting density $p(X(0))$, which we assume to be known. Writing Eq. (B5) in this way, we can effectively split the role of the input fields θ from those of the binary variables $X(t)$. We can think of Eq. (B5) as a reordering of the averages: starting with a known density $p(X(0))$, we compute the sum over the $X(0)$, which gives us a statistic of the $\theta(0)$ variables. We then integrate over $\theta(0), \hat{\theta}(0)$ to get the statistic of the $X(1)$, and then again sum over the $X(1)$ to get the statistic of the $\theta(1), \hat{\theta}(1)$, and so on. In practice however, these computations are not done exactly. In the following, we will specify the expansion which allows us to compute averages $\rho^\alpha(t)$ perturbatively.

First, observe that up to a prefactor $-i$, $\hat{\theta}_i(t)$ couples to $h_i(t)$ in the same manner as the source fields ψ couple to the physical observables X . We hence introduce another average

$$\rho_{\hat{\theta}_i}(t) = \langle \hat{\theta}_i(t) \rangle = -i \partial_{h_i(t)} W(\psi, h) \Big|_{\psi=0} = 0, \quad (\text{B6})$$

which vanishes due to the normalization condition on $W(\psi, h)$. We then use Eq. (B4) and Eq. (B6) to define the Legendre-Fenchel transform of Eq. (B3), which we will refer to as the effective action, via

$$\Gamma(\rho, \rho_{\hat{\theta}}) = \sup_{\psi, h} \psi^\top \rho - i h^\top \rho_{\hat{\theta}} - \mathcal{W}(\psi, h). \quad (\text{B7})$$

Together with Eq. (B4) and Eq. (B6), this yields the equations of state

$$\begin{aligned} \partial_{\rho_i^\alpha(t)} \Gamma(\rho, \rho_{\hat{\theta}}) &= \psi_i^\alpha(t) \\ \partial_{\rho_{\hat{\theta}_i}(t)} \Gamma(\rho, \rho_{\hat{\theta}}) &= -i h_i(t). \end{aligned} \quad (\text{B8})$$

To obtain the correction to the mean-field theory, we then proceed to expand Eq. (B7) to second order in β around the non-interacting case $\beta = 0$,

$$\Gamma \approx \Gamma_{\beta=0} + \beta \partial_\beta \Gamma + \frac{1}{2} \beta^2 \partial_\beta^2 \Gamma. \quad (\text{B9})$$

Reinserting this into Eq. (B8), to first order in β , one obtains the mean-field approximation Eq. (3), and the dynamical TAP equation Eq. (4) to second order.

We will now perform the expansion of Γ to second order in β term by term.

1. Noninteracting system

At $\beta = 0$, the cumulant generating function decomposes into a sum, since X_i, X_j are now independent for $i \neq j$,

$$\mathcal{W}_{\beta=0}(\psi, h) = \sum_i \ln Z_i(\psi_i, h_i), \quad (\text{B10})$$

we can view the terms $Z_i(t)$ as single-agent partition functions.

We must find Eq. (B7) under the conditions (B6), and (B4). To this end, we must express the fields ψ, h as functions of the mean values $\rho_i^\alpha, \rho_{\hat{\theta}}$. In the non-interacting case, the full information about the distribution of each of the binary variables at any time point is contained in their mean. This is so, because the variables are independent and binary, so that the individual means determine the entire distribution. The Markov property of the random process, the property that the present time step depends only on the previous one and not on its history, neither on future time

steps further allows us to write down the moment generating function of a single time step from t to $t+1$ with the averages at t given. We then have

$$\begin{aligned} Z_i(\psi_i, h_i) = & e^{\psi_i^S(t+1)} \underbrace{\rho_i^S(t)}_{S \rightarrow S} [1 - \phi(h_i(t))] \\ & + e^{\psi_i^I(t+1)} \left[\underbrace{\phi(h_i(t))\rho_i^S(t)}_{S \rightarrow I} + \underbrace{(1-\mu)\rho_i^I(t)}_{I \rightarrow I} \right] \\ & + \underbrace{\mu\rho_i^I(t)}_{I \rightarrow R} + \underbrace{1 - \rho_i^S(t) - \rho_i^I(t)}_{R \rightarrow R}. \end{aligned}$$

We have labeled the transition probabilities by the transitions in brackets, e.g. $S \rightarrow I$ for the transition from a susceptible to infected state. We must now find Eq. (B7) under the conditions Eq. (B6), Eq. (B4). We first evaluate Eq. (B6) from Eq. (B10)

$$\rho_{\hat{\theta}_i}(t) = \frac{-i\partial_{h_i(t)} Z_i(\psi_i, h_i)}{Z_i(\psi_i, h_i)} = \frac{-i\phi'(h_i(t))\rho_i^S(t) (e^{\psi_i^I(t+1)} - e^{\psi_i^S(t+1)})}{Z_i(\psi_i, h_i)} = 0,$$

hence we find for $\phi'(h_i(t))\rho_i^S(t) \neq 0$ that $\psi_i^I(t) = \psi_i^S(t) \forall i, t$. The derivatives by the sources ψ^S and ψ^I yield

$$\begin{aligned} \rho_i^S(t+1) &= \frac{e^{\psi_i^S(t+1)} [1 - \phi(h_i(t))] \rho_i^S(t)}{Z_i(t)} \\ \rho_i^I(t+1) &= \frac{e^{\psi_i^I(t+1)} (\phi(h_i(t))\rho_i^S(t) + (1-\mu)\rho_i^I(t))}{Z_i(t)} \end{aligned}$$

we solve these equations for $\psi_i^S(t), h_i(t)$, and obtain

$$\begin{aligned} \psi_i^S(t) &= \ln \frac{\rho_i^S(t) + \rho_i^I(t)}{1 - \rho_i^S(t) - \rho_i^I(t)} - \ln \frac{\rho_i^S(t-1) + (1-\mu)\rho_i^I(t-1)}{1 - \rho_i^S(t-1) - (1-\mu)\rho_i^I(t-1)} \\ h_i(t) &= \phi^{-1} \left(\frac{\rho_i^I(t+1)\rho_i^S(t) - \rho_i^S(t+1)(1-\mu)\rho_i^I(t)}{\rho_i^S(t+1)\rho_i^S(t) + \rho_i^I(t+1)\rho_i^S(t)} \right). \end{aligned}$$

We insert this back into Z , to obtain for the partition function

$$Z_i(\psi_i, h_i) = \prod_t \frac{(1 - \rho_i^S(t) - (1-\mu)\rho_i^I(t))}{1 - \rho_i^S(t+1) - \rho_i^I(t+1)}.$$

This quantity must equal one, since the partition function is normalized. This equation then simply expresses that the probability $1 - \rho_i^S(t) - \rho_i^I(t)$ that node i is recovered, increases by $\mu\rho_i^I(t)$ in each time step.

2. Mean-field

We will now compute the first order correction to Γ . To do so, we write

$$\Gamma = \ln \sum_X \rho(X(0)) \prod_{i,t} \int \frac{d\theta_i(t) d\hat{\theta}_i(t)}{2\pi} \exp(\Omega_\beta) W_{t+1,t} [X(t+1) | \theta(t), X(t)]$$

with Ω_β defined by

$$\begin{aligned} \Omega_\beta = \sum_{i,t} \left[\psi_i(t)^\top (\rho_i(t) - X_i(t)) + ih_i(t) (\hat{\theta}_i(t) - \rho_{\hat{\theta}_i}(t)) \right. \\ \left. - i\hat{\theta}_i(t) \left(\theta_i(t) - \beta \sum_j a_{ij} I_j(t) \right) \right]. \end{aligned} \tag{B11}$$

We may now use that, similar to the cumulant generating function, the derivative yields another average $\partial_\beta \Gamma = \langle \partial_\beta \Omega_\beta \rangle$. In the case that $\beta = 0$, all averages belonging to different indices factorize, because nodes i, j are independent for $i \neq j$. We hence find that

$$\begin{aligned} \partial_\beta \Gamma|_{\beta=0} &= \langle \partial_\beta \Omega_\beta \rangle|_{\beta=0} \\ &= i \sum_{i,t} \rho_{\hat{\theta}_i}(t) \sum_j a_{ij} \rho_j^I(t). \end{aligned}$$

To first order therefore, the effective action reads

$$\begin{aligned} \Gamma = \sum_{i,t} \left[\ln \left(\frac{1 - \rho_i^S(t+1) - \rho_i^I(t+1)}{(1 - \rho_i^S(t) - (1 - \mu)\rho_i^I(t))} \right) \right. \\ + (\rho_i^S(t) + \rho_i^I(t)) \left(\ln \frac{\rho_i^S(t) + \rho_i^I(t)}{1 - \rho_i^S(t) - \rho_i^I(t)} + \ln \frac{1 - \rho_i^S(t-1) - (1 - \mu)\rho_i^I(t-1)}{\rho_i^S(t-1) + (1 - \mu)\rho_i^I(t-1)} \right) \\ - i \rho_{\hat{\theta}_i}(t) \phi^{-1} \left(\frac{\rho_i^I(t+1)\rho_i^S(t) - \rho_i^S(t+1)(1 - \mu)\rho_i^I(t)}{\rho_i^S(t)(\rho_i^S(t+1) + \rho_i^I(t+1))} \right) \\ \left. + i \rho_{\hat{\theta}_i}(t) \beta \sum_j a_{ij} \rho_j^I(t) \right] + \mathcal{O}(\beta^2) \end{aligned} \quad (\text{B12})$$

To obtain the mean-field equation, we must take the derivative after $\rho_i(t), \rho_{\hat{\theta}_i}(t)$ and set the right hand side to zero. We find that both identities in Eq. (B8) are solved by

$$\rho_i^S(t) + \rho_i^I(t) = \rho_i^S(t-1) + (1 - \mu)\rho_i^I(t-1).$$

Taking the derivative by $\rho_{\hat{\theta}_i}(t)$ then yields the mean-field equations

$$\begin{aligned} \Delta \rho_i^S(t+1) &= -\rho_i^S(t) \phi \left(\beta \sum_j a_{ij} \rho_j^I(t) \right) \\ \Delta \rho_i^I(t+1) &= -\mu \rho_i^I(t) + \rho_i^S(t) \phi \left(\beta \sum_j a_{ij} \rho_j^I(t) \right). \end{aligned}$$

With ϕ the identity, we arrive at Eq. (3).

3. Second order correction

We compute the second derivative of Γ

$$\partial_\beta^2 \Gamma|_{\beta=0} = \left\langle \partial_\beta^2 \Omega_\beta \right\rangle_{\beta=0} + \left\langle (\partial_\beta \Omega_\beta)^2 \right\rangle_{\beta=0} - \left\langle \partial_\beta \Omega_\beta \right\rangle_{\beta=0}^2. \quad (\text{B13})$$

The first term vanishes. We are left with the variance of $\partial_\beta \Omega_\beta$ in the non-interacting case. Since we are at second order, the external fields acquire a linear dependence on β via their dependence on expectation values $\rho_i^\alpha, \rho_{\hat{\theta}}$. We must therefore consider derivatives of the type $\partial_\beta \psi_i^\alpha(t) = \partial_\beta \partial_{\rho_i^\alpha(t)} \Gamma$ and $\partial_\beta h_i(t) = i \partial_\beta \partial_{\rho_{\hat{\theta}_i}(t)} \Gamma$:

$$\partial_\beta \Omega_\beta - \langle \partial_\beta \Omega_\beta \rangle_{\beta=0} = i \sum_{i,j,t} a_{ij} \delta \hat{\theta}_i(t) \delta I_j(t), \quad (\text{B14})$$

where we define $\delta \hat{\theta}_i(t) = \hat{\theta}_i(t) - \rho_{\hat{\theta}_i}(t)$ and $\delta I_j(t) = I_j(t) - \rho_j^I(t)$. Evaluating the averages at $\beta = 0$ again means that all nodes of unequal indices can be treated independently. In the following, we will always evaluate expectation values in the non-interacting case and drop the subscript $\beta = 0$ for brevity. We hence arrive at

$$\partial_\beta^2 \Gamma|_{\beta=0} = - \sum_{t,t'} \sum_{ijkl} a_{ij} a_{kl} \left\langle \delta \hat{\theta}_i(t) \delta \hat{\theta}_k(t') \delta I_j(t) \delta I_l(t') \right\rangle. \quad (\text{B15})$$

If all indices i, \dots, l are unequal, then the term under the sum vanishes, since all nodes decouple. We must therefore have at least two indices equal to get a meaningful contribution.

We now go through the combinations of indices to determine which yield a meaningful contribution. We immediately observe that due to the prefactor of $a_{ij}a_{kl}$, we must have that $i \neq j$ and $k \neq l$. Due to this, the average in Eq. (B15) must always decompose into at least two factors. Furthermore, in each factor, each index must be equal to at least one other index, otherwise the term is proportional to $\langle \delta \hat{\theta} \rangle = 0$ or $\langle \delta I \rangle = 0$. From the latter two observations it follows that exactly two independent indices are left, thus the average in Eq. (B15) composes into exactly two factors. Thus we must either pair a factor of $\delta \hat{\theta}$ with another factor $\delta \hat{\theta}$ with the same node index, or a pair a factor of $\delta \hat{\theta}$ with another factor δI with the same node index. From

$$\langle \delta \hat{\theta}_i(t) \delta \hat{\theta}_i(t') \rangle = 0 \quad \forall i, t, t' \quad (\text{B16})$$

it follows that only the term where $i = l$ and $k = j$ remains, where each factor of $\delta \hat{\theta}$ is paired another factor δI with the same node index.

All in all, we find

$$\partial_\beta^2 \Gamma_{\beta=0} = - \sum_{t, t'} \sum_{ij} a_{ij} a_{ji} \langle \delta \hat{\theta}_i(t) \delta I_i(t') \rangle \langle \delta \hat{\theta}_j(t') \delta I_j(t) \rangle. \quad (\text{B17})$$

We must therefore compute expectation values of the form $\langle \hat{\theta}_i(t) I_i(t') \rangle$. We will see in the following that $\langle \hat{\theta}_i(t) I_i(t') \rangle$ vanishes unless $t < t'$. This is so, because $\langle \hat{\theta}_i(t) I_i(t') \rangle$ has the role of a response function: it measures the effect of a change in the field $h_i(t)$ at time t on the random variable $I_i(t')$ at another time point. In the case $t \geq t'$, therefore, we find that the factor in Eq. (B13) simplifies to

$$\begin{aligned} \langle \delta \hat{\theta}_i(t) \delta I_i(t') \rangle &= \langle \hat{\theta}_i(t) I_i(t') \rangle - \rho_{\hat{\theta}_i}(t) \rho_i^I(t') \\ &\stackrel{t \geq t'}{=} -\rho_{\hat{\theta}_i}(t) \rho_i^I(t'). \end{aligned}$$

Since the stochastic process is causal (later changes in the external field can have no influence on earlier time points), the response function is causal as well, and vanishes for $t \geq t'$. To evaluate the response function, we only need to consider the generating function from t to t' with the averages at $t-1$ given. Again, this is because of the Markov property of the random process.

For $\beta = 0$, it suffices to write down the moment generating function for a single node i :

$$\begin{aligned} Z_i(\psi_i, h_i) &= \rho_i^S(t) \left[\prod_{\tau=t}^{t'-1} [1 - \phi(h_i(\tau))] e^{\psi_i^S(\tau+1)} \right. \\ &\quad + \sum_{t_{\text{inf}}=t}^{t'-1} \phi(h_i(t_{\text{inf}})) e^{\psi_i^I(t_{\text{inf}}+1)} \left\{ \prod_{\tau=t}^{t_{\text{inf}}-1} [1 - \phi(h_i(\tau))] e^{\psi_i^S(\tau+1)} \right\} \\ &\quad \cdot \left\{ \prod_{\nu=t_{\text{inf}}+1}^{t'-1} [(1-\mu)e^{\psi_i^I(\nu+1)}] + \sum_{t_{\text{rec}}=t_{\text{inf}}+1}^{t'-1} \mu \prod_{\nu=t_{\text{inf}}+1}^{t_{\text{rec}}} [(1-\mu)e^{\psi_i^I(\nu+1)}] \right\} \\ &\quad + \rho_i^I(t) \left\{ \prod_{\nu=t}^{t'-1} [(1-\mu)e^{\psi_i^I(\nu+1)}] + \sum_{t_{\text{rec}}=t}^{t'-1} \mu \prod_{\nu=t}^{t_{\text{rec}}} [(1-\mu)e^{\psi_i^I(\nu+1)}] \right\} \\ &\quad \left. + 1 - \rho_i^S(t) - \rho_i^I(t) \right] \quad (\text{B18}) \end{aligned}$$

This sum is organized as follows: The first line corresponds to the node remaining susceptible. The second line counts all possible times t_{inf} of infection. The the first term in the third line corresponds to a remaining infection until t' . The second term counts all possible recovery times respectively. The fourth line counts all trajectories with initial infection, and respectively the possibilities of recovery, analogous to the third line. The last line corresponds to the node beginning in the recovered state. To compute $\langle \hat{\theta}_i(t) I_i(t') \rangle$, we take the derivative

$$\begin{aligned} \langle \hat{\theta}_i(t) I_i(t') \rangle_{\beta=0} &\stackrel{t' \geq t}{=} \left. \frac{-i \partial_{h_i(t)} \partial_{\psi_i^I(t')} Z_i(\psi_i, h_i)}{Z_i(\psi_i, h_i)} \right|_{\psi=h=0} \\ &= -i \rho_i^S(t) (1-\mu)^{t'-t-1}. \quad (\text{B19}) \end{aligned}$$

Where we used $\phi(0) = 0$, $\phi'(0) = 1$. Observe that the derivative in Eq. (B19) picks out of all possible trajectories precisely the one which corresponds an infection of node i at time point t , which lasts until time point t' with probability $(1 - \mu)^{t' - t - 1}$. For $t' < t$, no such trajectory exists, hence $\langle \hat{\theta}_i(t') I_i(t) \rangle = 0$. Therefore the product of the two averages always vanishes

$$\langle \hat{\theta}_k(t') I_k(t) \rangle \langle \hat{\theta}_i(t) I_i(t') \rangle = 0 \quad \forall i, k, t, t'. \quad (\text{B20})$$

Altogether, we have

$$\begin{aligned} \partial_{\beta}^2 \Gamma|_{\beta=0} = & - \sum_{t, t'} \sum_{ij} a_{ij} a_{ji} \left(2i \Theta(t - t') \rho_j^S(t') (1 - \mu)^{t - t' - 1} \rho_{\hat{\theta}_i}(t) \rho_i^I(t') \right. \\ & \left. + \rho_{\hat{\theta}_i}(t) \rho_i^I(t') \rho_{\hat{\theta}_j}(t') \rho_j^I(t) \right) \end{aligned} \quad (\text{B21})$$

From which we can compute second order correction to Eq. (B12). The correction only changes the equation of state originating from the derivative after $\rho_{\hat{\theta}}(t)$. This is so, because the factor $\rho_{\hat{\theta}}(t') = 0$ cancels all contributions of the correction term to the equation of state. The only relevant contribution to the equation of state is hence the term linear in $\rho_{\hat{\theta}}(t)$. All equations of state together finally yield Eq. (4).

Appendix C: Extension to SIS and SIRS model

We now extend the calculation to for the SIS and SIRS model. Up to (B5), the calculations remain unchanged, but now we must specify a different update probability

$$\begin{aligned} W_{t+1, t} [X(t+1) | \theta(t), X(t)] = & \prod_{i=1}^N \{ S_i(t+1) ([1 - \phi(\theta_i(t))] S_i(t) + \eta R_i(t) + \bar{\mu} I_i(t)) \\ & + I_i(t+1) [(1 - \mu - \bar{\mu}) I_i(t) + \phi(\theta_i(t)) S_i(t)] \\ & + R_i(t+1) [(1 - \eta) R_i(t) + \mu I_i(t)] \}, \end{aligned}$$

where now $\bar{\mu}$ is the probability for $I \rightarrow S$ and η for $R \rightarrow S$ and we used $R_i(t) = 1 - S_i(t) - I_i(t)$. We obtain the SIS model by setting $\mu = \eta = 0$. We set $\bar{\mu} = 0$ to obtain the the SIRS model.

1. Noninteracting case

We first compute $\Gamma|_{\beta=0}$. We again first compute the dependence of the sources on the averages. The derivatives by the sources ψ^S and ψ^I yield

$$\begin{aligned} \rho_i^S(t+1) &= \frac{e^{\psi_i^S(t+1)} [(1 - \phi(h_i(t)) - \eta) \rho_i^S(t) + \eta + (\bar{\mu} - \eta) \rho_i^I(t)]}{Z_i(t)} \\ \rho_i^I(t+1) &= \frac{e^{\psi_i^I(t+1)} (\phi(h_i(t)) \rho_i^S(t) + (1 - \mu - \bar{\mu}) \rho_i^I(t))}{Z_i(t)}. \end{aligned}$$

From the derivative by h , we again find that $\psi^S = \psi^I$. We solve these equations for $\psi_i^S(t)$, $h_i(t)$, and obtain

$$\begin{aligned} \psi_i^S(t) &= \ln \frac{\rho_i^S(t+1) + \rho_i^I(t+1)}{\rho_i^S(t) + \rho_i^I(t) + \eta (1 - \rho_i^S(t) - \rho_i^I(t)) - \mu \rho_i^I(t)} + \ln \frac{(1 - \eta) (1 - \rho_i^S(t) - \rho_i^I(t)) + \mu \rho_i^I(t)}{1 - \rho_i^S(t+1) - \rho_i^I(t+1)} \\ h_i(t) &= \phi^{-1} \left(\frac{-(1 - \mu - \bar{\mu}) \rho_i^S(t+1) \rho_i^I(t) + \rho_i^I(t+1) (\eta + (1 - \eta) \rho_i^S(t) + (\bar{\mu} - \eta) \rho_i^I(t))}{\rho_i^S(t) (\rho_i^S(t+1) + \rho_i^I(t+1))} \right). \end{aligned}$$

We insert this back into Z , to obtain for the partition function

$$Z_i(\psi_i, h_i) = \prod_t \frac{(1 - \eta) (1 - \rho_i^S(t) - \rho_i^I(t)) + \mu \rho_i^I(t)}{1 - \rho_i^S(t+1) - \rho_i^I(t+1)}.$$

This quantity must equal one, since the partition function is normalized. This equation then simply expresses that the probability $1 - \rho_i^S(t) - \rho_i^I(t)$ that node i is recovered, changes by $\mu \rho_i^I(t) - \eta (1 - \rho_i^S(t) - \rho_i^I(t))$ in each time step.

2. Mean-field equations

The mean-field equations follow analogously to Section B 2. We first take the derivative

$$\begin{aligned}\partial_\beta \Gamma|_{\beta=0} &= \langle \partial_\beta \Omega_\beta \rangle|_{\beta=0} \\ &= i \sum_{i,t} \rho_{\hat{\theta}_i}(t) \sum_j a_{ij} \rho_j^I(t),\end{aligned}$$

yielding the same contribution to Γ as for the SIR model. To first order therefore, the effective action reads

$$\begin{aligned}\Gamma = \sum_{i,t} \left[\ln \left(\frac{1 - \rho_i^S(t+1) - \rho_i^I(t+1)}{(1-\eta)(1-\rho_i^S(t) - \rho_i^I(t)) + \mu \rho_i^I(t)} \right) \right. \\ + (\rho_i^S(t) + \rho_i^I(t)) \left(\ln \frac{\rho_i^S(t+1) + \rho_i^I(t+1)}{\rho_i^S(t) + \rho_i^I(t) + \eta(1-\rho_i^S(t) - \rho_i^I(t)) - \mu \rho_i^I(t)} + \ln \frac{(1-\eta)(1-\rho_i^S(t) - \rho_i^I(t)) + \mu \rho_i^I(t)}{1 - \rho_i^S(t+1) - \rho_i^I(t+1)} \right) \\ - i \rho_{\hat{\theta}_i}(t) \phi^{-1} \left(\frac{-(1-\mu-\bar{\mu})\rho_i^S(t+1)\rho_i^I(t) + \rho_i^I(t+1)(\eta + (1-\eta)\rho_i^S(t) + (\bar{\mu}-\eta)\rho_i^I(t))}{\rho_i^S(t)(\rho_i^S(t+1) + \rho_i^I(t+1))} \right) \\ \left. + i \rho_{\hat{\theta}_i}(t) \beta \sum_j a_{ij} \rho_j^I(t) \right] + \mathcal{O}(\beta^2).\end{aligned}\tag{C1}$$

To obtain the mean-field equation, we must take the derivative after $\rho_i(t), \rho_{\hat{\theta}_i}(t)$ and set the right hand side to zero. We find that both identities in Eq. (B8) are solved by

$$\rho_i^S(t) + \rho_i^I(t) = \rho_i^S(t-1) + (1-\mu)\rho_i^I(t-1) + \eta(1-\rho_i^S(t-1) - \rho_i^I(t-1)).$$

Taking the derivative by $\rho_{\hat{\theta}_i}(t)$ then yields the mean-field equations

$$\begin{aligned}\Delta \rho_i^S(t+1) &= \eta(1-\rho_i^S(t) - \rho_i^I(t)) + \bar{\mu}\rho_i^I(t) - \rho_i^S(t) \phi \left(\beta \sum_j a_{ij} \rho_j^I(t) \right) \\ \Delta \rho_i^I(t+1) &= -(\mu + \bar{\mu})\rho_i^I(t) + \rho_i^S(t) \phi \left(\beta \sum_j a_{ij} \rho_j^I(t) \right).\end{aligned}$$

which now contain the transitions $I \rightarrow S$ and $R \rightarrow S$ with finite probability.

3. Second order correction

We proceed in the same fashion as in Appendix B 3, and again find that we must compute the moments in Eq. (B17). We first compute the correlation $\langle I_i(t)I_i(t') \rangle_{\beta=0}$. Because we evaluate this at $\beta = 0$, this moment corresponds to a sustained infection between the two time points, which occurs with probability

$$\langle I_i(t)I_i(t') \rangle_{\beta=0} \stackrel{t' \geq t}{=} (1-\mu-\bar{\mu})^{t'-t} \rho_i^I(t),$$

where now the rate at which the infection decays is $\mu + \bar{\mu}$. Similarly, the response function is

$$\langle \hat{\theta}_i(t)I_i(t') \rangle_{\beta=0} = -i \begin{cases} \rho_i^S(t)(1-\mu-\bar{\mu})^{t'-t-1} & t' > t \\ 0 & t' < t \end{cases}.$$

In principle, trajectories with multiple re-infections between time points t and t' must be taken into account to compute the average $\langle \hat{\theta}_i(t)I_i(t') \rangle$, since the transition $I \rightarrow S \rightarrow I$ and $I \rightarrow R \rightarrow S \rightarrow I$ are now allowed. But these terms drop out when we set $\beta = 0$. Finally, we have

$$\langle \hat{\theta}_i(t)\hat{\theta}_i(t') \rangle = 0,$$

due to the normalization, as before. We therefore find that the second order correction yields the same terms as for the SIR model, when we replace $\mu \rightarrow \mu + \bar{\mu}$. The final update equation reads (with ϕ the identity)

$$\begin{aligned}\Delta\rho_i^S(t+1) &= \eta(1 - \rho_i^S(t) - \rho_i^I(t)) + \bar{\mu}\rho_i^I(t) - \rho_i^S(t)\beta\sum_j a_{ij}(\rho_j^I(t) - \rho_{j\leftarrow i}^I(t)) \\ \Delta\rho_i^I(t+1) &= -(\mu + \bar{\mu})\rho_i^I(t) + \rho_i^S(t)\beta\sum_j a_{ij}(\rho_j^I(t) - \rho_{j\leftarrow i}^I(t)).\end{aligned}$$

with the self-feedback correction

$$\rho_{j\leftarrow i}^I(t) := \beta a_{ji} \sum_{t' \leq t-1} \rho_j^S(t') \rho_i^I(t') (1 - \mu - \bar{\mu})^{t-t'-1}.$$

Setting $\bar{\mu}$ to zero, one obtains the equation for the SIRS model, and setting μ, η to zero, one obtains the update equation for the SIS model. These equations are stated explicitly in Table I.

Appendix D: Epidemic dynamics in a Spiking Simulator code

We implement the dynamics of the SIR, SIRS and SIS model in NEST [16], a simulator for spiking neurons. NEST has previously been used to model binary neurons [26]. We here follow the same approach as in [26] to adapt the simulator to the SIR, SIRS, and SIS dynamics.

Note that each agent i needs not know the exact state of its nearest neighbors to compute the update probability, rather, it suffices to know how many of these nearest neighbors are infected. This information is encoded in the input θ_i to the agent. We use spikes to transmit changes to these fields: When an agent i is infected, it sends out a spike. Upon receiving a spike, the nearest neighbors j of the agent hence increments their input fields θ_j by β . When agent i leaves the infected state, it sends two spikes at the same time. Two simultaneous spikes received by a nearest neighbor j then result in a reduction of θ_j by β . The implementation will be released as open source with one of the forthcoming releases of the simulator.

Appendix E: Mean-field and TAP solutions

We compute the predictions from mean-field and TAP solutions using Eq. (3) for mean-field and the corresponding set of coupled differential equations for TAP in Table I. At the beginning of each simulation, a random subset of agents is infected, for these we set $\rho_i^S(0) = 0$, and $\rho_i^I(0) = 1$, while for all other agents we set $\rho_i^S(0) = 1$, and $\rho_i^I(0) = 0$. We also set $\tau_i(0) = 0$ for all agents for the TAP approximation. Within the TAP approximation, values of $\theta_i(t)$ outside the $[0, 1]$ interval can occur, we hence use a cutoff function $\phi(\theta) = \max(0, \min(1, \theta))$ as indicated in Section II to reset the value of θ back to the closest physical value. We then compute the average fraction of individuals in the state α reported in Fig. 2, Fig. 3 and Fig. 4 by summing, $\rho^\alpha(t) = \frac{1}{N} \sum_i \rho_i^\alpha(t)$.

Appendix F: Predictions for the epidemic threshold

We will now compute how the endemic state depends on the network topology and the rates of infection and recovery. The epidemic threshold bears a resemblance to a phase transition: at a certain parameter λ , the system properties fundamentally change: the absorbing state, where the number of infected agents is zero, becomes unstable. Rather, the number of infected agents increases. Before we derive the epidemic threshold from Eq. (4), we state three known estimates for the epidemic threshold originating from mean-field theory. We will here find that all three estimates from the TAP equations are the same independent of whether one chooses the SIS or SIRS model.

Individual-based mean-field theory, also referred to as quenched mean-field theory, corresponds to the evolution equations (3) [20]. Linearizing these equations for small initial infection levels yields the condition

$$\lambda_c^{\text{IBMF}} = \lambda_{a, \max}^{-1} \quad (\text{F1})$$

with $\lambda_{A, \max}$ the largest eigenvalue of the adjacency matrix. If λ is larger than this value, the number of infected agents will grow according to Eq. (3).

Degree-based mean-field theory, which stipulates that all agents of equal degree are statistically equivalent, yields the following result [27]

$$\lambda_c^{\text{DBMF}} = \frac{\langle k \rangle}{\langle k^2 \rangle} \quad (\text{F2})$$

provided that the network has an uncorrelated degree distribution: the probability $p(k'|k)$ that a node of degree k is connected to a node of degree k' is $p(k')k'/\langle k \rangle$.

DMP For $\gamma \leq \frac{5}{2}$, degree-based mean-field theory and individual-based mean-field theory are expected to yield equivalent results for large N [20]. For $\gamma > \frac{5}{2}$, individual-based mean-field theory is known to overestimate the epidemic threshold. This coincides with the point where the largest eigenvalue of the adjacency matrix localizes due to the self-feedback effect, see [28]. The authors of Ref. [28] suggest that to assess the relative importance of a node in a graph, the leading eigenvector of the following matrix $2N \times 2B$ should be considered

$$M = \begin{pmatrix} a & \mathbb{1} - K \\ \mathbb{1} & 0 \end{pmatrix}, \quad (\text{F3})$$

where $K_{ij} = \delta_{ij}k_i$ is a diagonal matrix with the degree k_i of the node i on the diagonal. The underlying idea is that the self-feedback effect makes hubs appear more relevant than they are. This suggestion coincides with the estimator of the epidemic threshold for DMP. The estimator for the DMP epidemic threshold is then the inverse leading eigenvalue of M [23, 24]. We will see in the following, that the TAP estimation follows from a similar $2N \times 2N$ matrix, whose off-diagonal blocks however differ from those in M .

TAP prediction. We now compute an estimate for λ_c from Eq. (4). To simplify the analysis, we again define dynamical variable $\tau_i(t)$ which has the following properties

$$\begin{aligned} \tau_i(0) &= 0 \\ \Delta \tau_i(t+1) &= -(\mu + \bar{\mu})\tau_i(t) + \rho_i^I(t)\beta \sum_j a_{ij}a_{ji}\rho_j^S(t). \end{aligned}$$

Note that in comparison to the definition in the main text, Eq. (7), τ here decays with $\mu + \bar{\mu}$, to account for the SIS ($\mu = 0, \bar{\mu} > 0$) and the SIRS ($\bar{\mu} = 0, \mu > 0$) model at the same time. Using τ , we may write Eq. (4) as

$$\begin{aligned} \Delta \rho_i^I(t+1) &= -(\mu + \bar{\mu})\rho_i^I(t) + \rho_i^S(t)\beta \left(\sum_j A_{ij}\rho_j^I(t) - \tau_i(t) \right) \\ \Delta \rho_i^R(t+1) &= \mu\rho_i^I(t) - \eta\rho_i^R(t), \end{aligned}$$

and we further require that $\rho_i^S(t) = 1 - \rho_i^I(t)$ for the SIS and $\rho_i^S(t) = 1 - \rho_i^R(t) - \rho_i^I(t)$ for the SIRS model. We now examine the regime in which ρ^I is infinitesimally small, hence we keep only terms up to linear order in ρ^I . We also set ρ^R to zero in the case of the SIRS model. This can be seen as a small perturbation from the state of zero activity. If this state is unstable, the number of infected agents grows, $\Delta \rho^I > 0$, and we are above the epidemic threshold. Linearizing in ρ^I , we find that

$$\begin{aligned} \rho_i^I(t)\beta \sum_j a_{ij}a_{ji}\rho_j^S(t) &= \rho_i^I(t)\beta \sum_j a_{ij}a_{ji}(1 - \rho_j^I(t)) \\ &= \rho_i^I(t)\beta \sum_j a_{ij}^2 + \mathcal{O}\left((\rho^I(t))^2\right), \end{aligned}$$

where we used that $a = a^T$ in an undirected network. Finally, we can replace the sum $\sum_j a_{ij}^2 = k_i$ by the degree k_i of the i -th node. The linearized update equations hence read:

$$\begin{pmatrix} \Delta \vec{\rho}^I(t+1) \\ \Delta \vec{\tau}(t+1) \end{pmatrix} = \left[-(\mu + \bar{\mu}) \begin{pmatrix} \mathbb{1} & 0 \\ 0 & \mathbb{1} \end{pmatrix} + \beta \begin{pmatrix} a & -\mathbb{1} \\ K & 0 \end{pmatrix} \right] \begin{pmatrix} \vec{\rho}^I(t) \\ \vec{\tau}(t) \end{pmatrix}, \quad (\text{F4})$$

with $K_{ij} = \delta_{ij}k_i$ a diagonal matrix with the degrees of the nodes along the diagonal. We now ask that the right hand side of this equation must be equal to zero: This is exactly the point where the activity neither decays nor increases and therefore marks the transition point. This gives us an eigenvalue equation

$$\lambda^{-1} \begin{pmatrix} \rho^I(t) \\ \tau(t) \end{pmatrix} = \underbrace{\begin{pmatrix} a & -\mathbb{1} \\ K & 0 \end{pmatrix}}_{=:D} \begin{pmatrix} \rho^I(t) \\ \tau(t) \end{pmatrix}, \quad (\text{F5})$$

where we use $\lambda = \frac{\beta}{\mu}$ in case of the SIS and $\lambda = \frac{\beta}{\mu}$ for the SIRS model. The estimator for the epidemic threshold is hence

$$\lambda_c^{\text{TAP}} = (\lambda_D^{\text{max}})^{-1}, \quad (\text{F6})$$

the inverse leading eigenvalue of D . Since the matrix D is not symmetric, we can obtain complex eigenvalues, corresponding to oscillatory solutions to Eq. (F4). In the case of random regular graphs, a homogeneous ansatz for the eigenvector yields $(\lambda_D^{\text{max}})^{-1}_{\pm} = \frac{1}{2} \left(1 \pm \sqrt{1 - \frac{4}{k}} \right)$, consistent with the fixpoint analysis of the previous section. In the case of scale-free networks, treated in the next section, we found only real leading eigenvalues of D .

Appendix G: Epidemic threshold in scale-free networks

We now move to a different class of networks: scale-free networks. They are defined by having a degree distribution which follows $p(k) \sim k^{-\gamma}$. These networks are more heterogeneous: alongside many nodes of low degree, there are a number of hubs h with degree far above the network average $k_h \gg \langle k \rangle$; the proportion of these hubs in the population increases for smaller γ . Scale-free networks as contact graphs hence represent a more heterogeneous society, where few individuals have far more contacts than average. In this section, we present our results on the endemic activity in the SIRS model in scale-free networks.

We now compare these different approaches to each other on scale-free networks. We generate networks with scale-free distributions $p(k) \sim k^{-\gamma}, k \geq k_0$ using the configuration model [29]. To ensure that the networks are connected with high probability, we choose a minimal degree $k_0 = 3$. We then perform simulations of the SIRS model for various values of λ . The epidemic threshold is determined by finding the maximum of the susceptibility

$$\chi = N \frac{\langle (\rho^I)^2 \rangle - \langle \rho^I \rangle^2}{\langle \rho^I \rangle}, \quad (\text{G1})$$

where the average is computed in the endemic state, see e.g. [20].

Figure 5 shows a comparison of the three different predictions to simulations. We first compare the onset of activity in the endemic state ρ_{∞}^I , to TAP, degree-based mean-field (DBMF) and mean-field predictions in Fig. 5 a),b) for different system sizes and varying γ . We find that the TAP predictor most closely tracks the onset of the regime with finite endemic activity. We also compute χ for the same configurations, and find that it peaks at the same values of λ in Fig. 5 c), d). We then determine λ_c from the peak position of the susceptibility, and compare it to the different predictors for varying N in Fig. 5 (e)-(g). For small system sizes, the TAP theory yields the most accurate predictions. As the system size increases, degree-based mean-field theory and the TAP prediction yield more and more similar predictions. For $\gamma = 2.3$, all three theories eventually agree with the simulation, see Fig. 5 c). For $\gamma = 2.9$, individual-based and degree-based mean-field theory do not agree, as we expect. However, both the TAP estimator and the degree-based mean-field result show a good agreement with the simulation. This analysis also shows that the TAP prediction and dynamical message passing are not equivalent: dynamical message passing overestimates the epidemic threshold in the same parameter regime [23]. We hence see that although our theory eliminates self-feedback effects up to second order in β , it is not equivalent to DMP.

For $\gamma = 3.1$, we also find that the TAP theory produces a good estimate at small system sizes, see Fig. 5 g). For large system sizes, we find that the TAP predictor eventually converges to the result from degree-based mean-field theory, overestimating λ_c . We expect that this is due to terms of higher order in β , computing higher order corrections to the TAP result may improve the prediction.

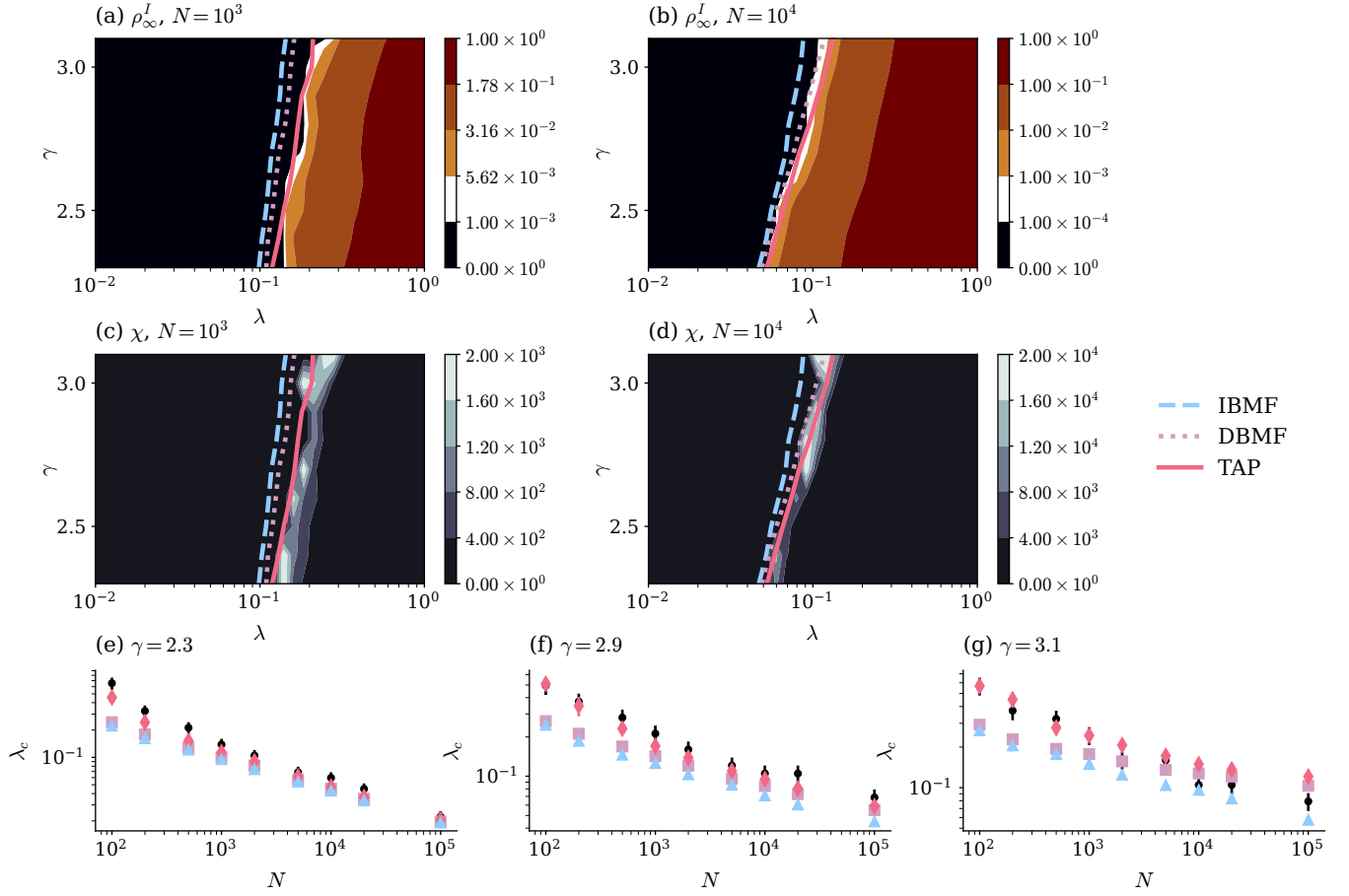


Figure 5. **Epidemic threshold for the SIRS model on scale free networks with $\eta = 0.1$.** (a) Shows the fraction of infected agents after the dynamics have reached an equilibrium state for varying λ and γ . Dashed curves stem from the mean-field predictions Eq. (F1), dotted from degree-based mean-field predictions Eq. (F2), and solid curves indicate the TAP prediction Eq. (F6). (b) Same as (a), but for larger system size. (c) Shows susceptibility, Eq. (G1), for scale free networks of size 10^3 . Curves again indicate the predictions for λ_c . (d) Same as (c) but for larger system sizes $N = 10^4$. (e) Black dots show λ_c from simulations over system size for $\gamma = 2.3$. Blue triangles, purple squares and pink diamonds show the predictions from individual-based mean-field theory, degree-based mean-field theory, and TAP respectively. (f) (g) Same as (c) but for $\gamma = 2.9$ and $\gamma = 3.1$, respectively. All simulation results in panels (a)-(g) stem from a single realization of the network connectivity per system size. Theoretical predictions (mean-field theory, degree-based mean-field theory, and TAP) were averaged over 10 different realizations of the connectivity.

-
- [1] W. O. Kermack and A. G. McKendrick, *Bulletin of Mathematical Biology* **53**, 33 (1991).
 - [2] S. Thurner, P. Klimek, and R. Hanel, *Proceedings of the National Academy of Sciences* **117**, 22684 (2020).
 - [3] M. L. Heltberg, C. Michelsen, E. S. Martiny, L. E. Christensen, M. H. Jensen, T. Halasa, and T. C. Petersen, *Royal Society Open Science* **9**, 220018 (2022).
 - [4] A. V. Tkachenko, S. Maslov, A. Elbanna, G. N. Wong, Z. J. Weiner, and N. Goldenfeld, *Proceedings of the National Academy of Sciences* **118**, e2015972118 (2021), arxiv:2008.08142 [physics, q-bio].
 - [5] M. E. J. Newman, *Physical Review E* **66**, 016128 (2002).
 - [6] Y. Moreno, R. Pastor-Satorras, and A. Vespignani, *The European Physical Journal B - Condensed Matter and Complex Systems* **26**, 521 (2002).
 - [7] R. M. May and A. L. Lloyd, *Physical Review E* **64**, 066112 (2001).
 - [8] R. Pastor-Satorras, C. Castellano, P. Van Mieghem, and A. Vespignani, *Reviews of Modern Physics* **87**, 925 (2015).
 - [9] Y. Roudi and J. Hertz, *Journal of Statistical Mechanics: Theory and Experiment* **2011**, P03031 (2011), arxiv:1103.1044 [cond-mat].

- [10] B. Karrer and M. E. J. Newman, *Physical Review E* **82**, 016101 (2010).
- [11] A. Y. Lokhov, M. Mézard, H. Ohta, and L. Zdeborová, *Physical Review E* **90**, 012801 (2014).
- [12] A. S. Mata and S. C. Ferreira, *Europhysics Letters* **103**, 48003 (2013).
- [13] T. Plefka, **15**, 1971 (1982).
- [14] D. J. Thouless, P. W. Anderson, and R. G. Palmer, **35**, 593 (1977).
- [15] A. N. Vasiliev and R. A. Radzhabov, **21**, 963 (1974).
- [16] M.-O. Gewaltig and M. Diesmann, *Scholarpedia* **2**, 1430 (2007).
- [17] M. Henkel, H. Hinrichsen, S. Lübeck, and M. Pleimling, *Non-Equilibrium Phase Transitions, Theoretical and Mathematical Physics* (Springer, Dordrecht [Netherlands] ; New York, 2008).
- [18] D. ben-Avraham and J. Köhler, *Physical Review A* **45**, 8358 (1992).
- [19] Y. Roudi, J. Tyrcha, and J. Hertz, **79**, 051915 (2009).
- [20] R. Pastor-Satorras, C. Castellano, P. Van Mieghem, and A. Vespignani, *Reviews of Modern Physics* **87**, 925 (2015).
- [21] A. V. Goltsev, S. N. Dorogovtsev, J. G. Oliveira, and J. F. F. Mendes, *Physical Review Letters* **109**, 128702 (2012).
- [22] C. Castellano and R. Pastor-Satorras, *Physical Review X* **10**, 011070 (2020).
- [23] C. Castellano and R. Pastor-Satorras, *Physical Review E* **98**, 052313 (2018).
- [24] M. Shrestha, S. V. Scarpino, and C. Moore, *Physical Review E* **92**, 022821 (2015).
- [25] J. C. M. Silva, D. H. Silva, F. A. Rodrigues, and S. C. Ferreira, *Physical Review E* **106**, 034317 (2022).
- [26] D. Grytskyy, T. Tetzlaff, M. Diesmann, and M. Helias, **7**, 131 (2013).
- [27] R. Pastor-Satorras and A. Vespignani, *Physical Review Letters* **86**, 3200 (2001).
- [28] T. Martin, X. Zhang, and M. E. J. Newman, *Physical Review E* **90**, 052808 (2014).
- [29] M. E. J. Newman, in *Handbook of Graphs and Networks* (John Wiley & Sons, Ltd, 2002) Chap. 2, pp. 35–68.